# An improved numerical integration method to predict the milling stability based on the Lagrange interpolation scheme

**Yan Xia[a, b], Yi Wan[a, b *], Xichun Luo[c], Zhanqiang Liu[a, b], Qinghua Song[a, b]**

[a] Key Laboratory of High Efficiency and Clean Mechanical Manufacture, Ministry of Education, School of Mechanical Engineering, Shandong University, Jinan, 250061, China

[b] National Demonstration Centre for Experimental Mechanical Engineering Education, Shandong University, Jinan, 250061, China

[c] Centre for Precision Manufacturing, DMEM, University of Strathclyde, Glasgow, G1 1XJ, UK

* Correspondence: wanyi@sdu.edu.cn

**Abstract:**

To predict the milling stability accurately and efficiently, an improved numerical integration method (INIM) is proposed based on the Lagrange interpolation scheme. First, the milling dynamic model considering the regenerative chatter can be described as a delay linear differential equation. The tooth passing period of the milling cutter is divided into the free and forced vibration stages. Then, the forced vibration stage is equally discretized, and the INIMs are built based on the Lagrange interpolation scheme within the discretized intervals to construct the state transition matrix. Finally, the convergence rates and the stability lobes for the benchmark milling systems are calculated and discussed by using the proposed INIMs and the existing methods, respectively. The comparison results reveal that the proposed second-order INIM shows higher computational efficiency and accuracy compared with the related discretization methods, and meantime it is more accurate under just slightly loss of the time cost compared with the existing NIMs.

**Keywords:**

Milling stability; Numerical integration method; Lagrange interpolation scheme; Convergence rate; Stability lobe diagram

## 1. Introduction

During cutting process, regenerative chatter frequently occurs, which will deteriorate the machining quality and productivity, and even damage the cutters and machine tool [1]. Till now, aimed at the chatter problem, a number of studies from the views of the chatter mechanism [2], chatter prediction [3, 4], chatter detection [5, 6], and chatter control [7, 8] have been doing. Due to the practical,



This is a peer-reviewed, accepted author manuscript of the following article: Xia, Y., Wan, Y., Luo, X., Liu, Z., & Song, Q. (2021). An improved numerical integration method to predict the milling stability based on the Lagrange interpolation scheme. International Journal of Advanced Manufacturing Technology . https://doi.org/10.1007/s00170-021-07311-z

efficient, and low-cost advantages, the chatter prediction has received much attention. Its essence is to achieve the chatter-free machining process by seeking the appropriate cutting parameters from the stability lobe diagram (SLD). In order to predict the SLD accurately and efficiently, lots of calculated methods have been put forward, mainly including frequency domain and time domain ones.

The zero-order approximation method was proposed to predict the SLD, where the Fourier series were used to estimate the milling force coefficients [9]. It was a very efficient approach but was not applicable to the low radial immersion condition. In order to overcome this shortcoming, the multi-frequency method (MFM) was explored subsequently [10]. Then, the MFM was further extended when the harmonics of both the tooth spacing angle and the tooth passing frequencies were taken into account [11]. The frequency method could be also used to solve the stability zone for the non-standard cutting tools with variable pitch and variable helix [12, 13].

Thanks to the advances in the computer technology, various numerical approaches in time domain were investigated. For instance, the time domain simulation method was developed to calculate the milling stability lobes [14]. The temporal finite element analysis (TFEA) was presented to determine the stability at the arbitrary time in the cut [15]. The chatter stability lobes in time domain were achieved using the numerical method [16]. Through approximating the delayed item, the zeroth-order and first-order semi-discretization methods (SDMs) were proposed respectively, where the tooth passing period was discretized equally [3, 17]. To further improve the computational accuracy, the second-order SDM then was investigated based on the Newton interpolation polynomial [18].

Inspired by the SDM, the full-discretization method (FDM) was built, where both the delayed item and the system state item were approximated by way of the linear interpolation [4]. Compared with the zeroth-order SDM, the first-order FDM converged faster. Subsequently, the improved FDMs with higher computational accuracy were put forward by using the higher-order interpolation polynomials [19-27]. As a result, the second-order Lagrange polynomial [19, 20], third-order Newton polynomial [21-24], and third-order Hermite polynomial [25, 26] were separately employed to estimate the system state item. Correspondingly, the delayed item was interpolated by the second-order or third-order Lagrange polynomial [20, 24, 25], the second-order Hermite polynomial [23],

and the third-order Newton polynomial [22, 26], respectively. Furthermore, the fourth-order and fifth-order methods were proposed to further increase the precision of the stability prediction [27, 28]. Although these higher order FDMs can achieve the high computational accuracy, the corresponding time cost increases with the increase of the interpolation order. In addition, a complete discretization scheme (CDS) was explored for predicting the milling stability based on the numerical iteration method, such as Euler's method, in which the delayed item, time domain item, parameter item, and the differential item were discretized [29]. The computational efficiency of the CDS was faster than the FDM, but its computational accuracy was lower due to the low truncation error of the Euler's method. Then, the updated CDS was proposed based on the classical Runge-Kutta method, and the computational accuracy was improved [30].

Based on the direct integration scheme of the FDM and the time period division form of the TFEA, many numerical integration methods (NIMs) were developed to achieve the chatter stability. The NIM was early proposed to predict the milling stability, where the Newton-Cotes and Gauss integration formulas were used to estimate the integral item respectively [31]. The calculated results showed that the NIM was highly efficient and accurate. The NIM could be employed to analyze the milling stability, which considered the structural mode coupling effect and regenerative effect simultaneously [32]. Subsequently, based on the Simpson integration formula, the Simpson method was developed to analyze the stability of milling operation, whose convergence rate was faster than the first-order SDM and second-order FDM [33]. A numerical differentiation method based on the Taylor series expansion was presented to predict the chatter stability as well [34]. According to the linear multistep method, the Milne-Simpson-based-corrector method was investigated to improve the calculated performance [35]. Additionally, other numerical methods were constructed using the Adams correlation formulas, such as Adams-Moulton-based method [36], Adams-Bashforth scheme [37], and the implicit Adams method [38].

From the mentioned references above, it can be found that a diverse range of methods for the chatter stability prediction are gradually proposed, whose common goal is to achieve the accurate and efficient prediction. In order to further improve the computational performance, an improved NIM is proposed based on the Lagrange interpolation scheme in this work. The reminder of the paper is organized as follows: Section 2 builds the mathematical model for the milling process with

the regenerative effect is taken into account. Then, in Section 3, the numerical integration formulas are constructed by means of the Lagrange interpolation scheme, and thus the INIMs are proposed. The optimal order for the INIM is determined in Section 4. Compared with the existing methods including the SDM, the FDMs and the NIMs, Section 5 verifies the effectiveness of the proposed INIM. Lastly, some conclusions are drawn in Section 6.

## 2. Mathematical model of milling process

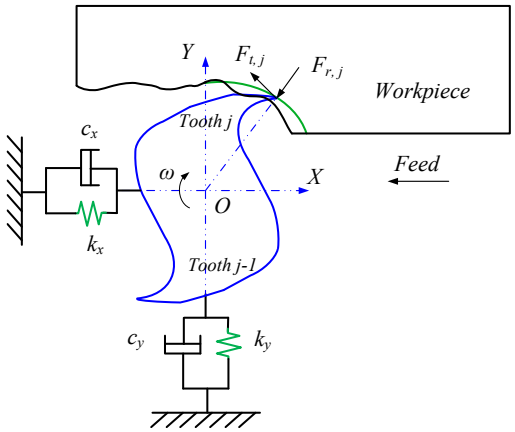


**Fig. 1** Dynamic models of milling process

Figure 1 shows the dynamic milling model with two degrees of freedom (DOF), where the regenerative effect is considered. Note, the linear dynamic model used in this paper is the same as those from Ref. [3, 4, 18-31, 33-36, 38], whereas the effects of some complex factors are neglected, such as the loss of contact effects, multiple regenerative effects and time-varying delays [39-44]. Here, the workpiece is assumed to be rigid, whereas the cutter is modeled as the flexible body. When the static milling force is neglected, since it won't affect the dynamic stability, the milling systems are generally characterized in physical space as follows:

$$\mathbf{M}\ddot{\mathbf{u}}(t)+\mathbf{C}\dot{\mathbf{u}}(t)+\mathbf{K}\mathbf{u}(t)=a_p\mathbf{K}_c(t)[\mathbf{u}(t)-\mathbf{u}(t-T)] \tag{1}$$

where **M**, **C** and **K** refer to the mass matrix, damping matrix, and stiffness matrix, respectively. $\mathbf{K}_c(t)$ is the periodic coefficient matrix, $a_p$ is the axial cutting depth, $T$ represents the time period. $\mathbf{u}(t)$ is the modal coordinate, which denotes $x(t)$ for the single DOF system and $[x(t)\ y(t)]^{\mathrm{T}}$ for the two DOFs system, respectively.

Introduce two vector notations $\mathbf{p}(t)$ and $\mathbf{q}(t)$:

$$\mathbf{p}(t)=\mathbf{M}\dot{\mathbf{u}}(t)+\mathbf{C}\mathbf{u}(t)/2 \quad \mathbf{q}(t)=[\mathbf{u}(t) \quad \mathbf{p}(t)]^T \tag{2}$$

Substituting Eq. (2) into Eq. (1) leads to

$$\dot{\mathbf{q}}(t)=\mathbf{A}\mathbf{q}(t)+a\mathbf{B}(t)[\mathbf{q}(t)-\mathbf{q}(t-T)] \tag{3}$$

with

$$\mathbf{A}=\begin{bmatrix} -\mathbf{M}^{-1}\mathbf{C}/2 & \mathbf{M}^{-1} \\ \mathbf{C}\mathbf{M}^{-1}\mathbf{C}/4-\mathbf{K} & -\mathbf{C}\mathbf{M}^{-1}/2 \end{bmatrix} \quad \mathbf{B}(t)=\begin{bmatrix} 0 & 0 \\ \mathbf{K}_c(t) & 0 \end{bmatrix}$$

where the matrices **A** and **B** for the single DOF or two DOFs milling systems are represented in the Appendix in detail.

According to the direct integration scheme [4], the response of Eq. (3) can be described as:

$$\mathbf{q}(t)=e^{\mathbf{A}(t-t_0)}\mathbf{q}(t_0)+a_{\mathrm{p}}\int_{t_0}^{t}\left\{e^{\mathbf{A}(t-\xi)}\mathbf{B}(\xi)\left[\mathbf{q}(\xi)-\mathbf{q}(\xi-T)\right]\right\}d\xi \tag{4}$$

In order to solve Eq. (4), the numerical integration formulas are constructed based on the Lagrange interpolation scheme in the next section.

## 3. Numerical algorithms

### 3.1 Construction of the numerical integration formulas

Assuming that a continuous function $f(x)$ exists at the interval $[a, b]$, and its values are $f(x_i)$, $f(x_{i+1})$, $f(x_{i+2})$… at the corresponding points $a \le x_i < x_{i+1} < x_{i+2} < x_{i+3} < \ldots \le b$, respectively. According to the Lagrange interpolation scheme, the $n$-order interpolation polynomial $L_n(x)$ of the function $f(x)$ can be obtained as:

$$\begin{aligned} L_n(x)&=\sum_{j=0}^{n} f(x_j)l_j(x) \qquad n=1, 2, 3, ... \\ l_j(x)&=\prod_{\substack{i=1 \\ i\neq j}}^{n}\frac{(x-x_i)}{(x_j-x_i)} \end{aligned} \tag{5}$$

Hence, when $n$ = 1 and 2, the interpolation formulas $L_{\mathrm{n}}(x)$ can be expressed as follows:

$$L_1(x)=\frac{x-x_{i+1}}{-h}f(x_i)+\frac{x-x_i}{h}f(x_{i+1}) \tag{6}$$

$$\begin{aligned} L_2(x)=&\frac{(x-x_{i+1})(x-x_{i+2})}{2h^2}f(x_i) \\ &-\frac{(x-x_i)(x-x_{i+2})}{h^2}f(x_{i+1}) \\ &+\frac{(x-x_i)(x-x_{i+1})}{2h^2}f(x_{i+2}) \end{aligned} \tag{7}$$

where $h = x_{i+1} - x_i = x_{i+2} - x_{i+1}$.

Integrating on the two sides of Eqs. (6) and (7) over the interval $[x_i, x_{i+1}]$, thus the corresponding

numerical integral formulas are respectively written as follows:

$$\int_{x_i}^{x_{i+1}} f(x)\,dx \approx \frac{h}{2}\left[f(x_i)+f(x_{i+1})\right] \tag{8}$$

$$\int_{x_i}^{x_{i+1}} f(x)\,dx \approx \frac{h}{12}\left[5f(x_i)+8f(x_{i+1})-f(x_{i+2})\right] \tag{9}$$

### 3.2 Improved numerical integration method (INIM)

Since the cutting teeth cuts in and off the workpiece periodically, the milling process is intermittent. When the tool enters into the workpiece, the cutting forces are dependent on the tool displacement, which generates the forced vibration; when out of the workpiece, the tool is not subjected to the cutting forces, which means the free vibration. That is to say, one tooth passing period $T$ can be divided into the free and the forced vibration intervals [15]. In Fig. 2, $T_f$ refers to the free vibration process, where $t_0$ and $t_1$ are the starting and ending points separately, and the rest time interval $T_u$ is forced vibration process. In order to describe the cutting region accurately, the forced vibration process is discretized equally with $T_u = m\tau$, where the discrete number $m$ is integral.

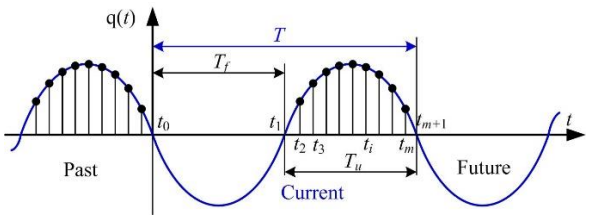


**Fig. 2** The discretization map of the tooth passing period during milling process

Thus, the arbitrary time point $t_i$ over one tooth passing period $T$ can be described as:

$$t_i = t_0 + T_f + (i-1)\tau, \quad i = 1, 2, \cdots, m+1 \tag{10}$$

where τ is the length of every small interval $[t_i, t_{i+1}]$.

#### 3.2.1 First-order INIM (1st INIM)

Since the time points $t_0$ and $t_1$ belong to the free vibration process, the value of $\boldsymbol{q}(t_1)$ in the Eq. (4) can be expressed as follows:

$$\mathbf{q}(t_1) = e^{\mathbf{A}T_f}\mathbf{q}(t_0) \tag{11}$$

Then, the time point $t_2$ is the start point of the forced vibration interval. Based on the first-order numerical integral formula in Eq. (8), $\boldsymbol{q}(t_2)$ of Eq. (4) can be obtained as:

$$\begin{aligned}\mathbf{q}(t_2) &= e^{\mathbf{A}(t_2-t_1)}\mathbf{q}(t_1) + a_p\int_{t_1}^{t_2} e^{\mathbf{A}(t_2-\xi)}\mathbf{B}(\xi)[\mathbf{q}(\xi)-\mathbf{q}(\xi-T)]d\xi \\ &= e^{\mathbf{A}(t_2-t_1)}\mathbf{q}(t_1) + \frac{\tau}{2}a_p\begin{Bmatrix} e^{\mathbf{A}(t_2-t_1)}\mathbf{B}(t_1)[\mathbf{q}(t_1)-\mathbf{q}(t_1-T)]+ \\ \mathbf{B}(t_2)[\mathbf{q}(t_2)-\mathbf{q}(t_2-T)] \end{Bmatrix}\end{aligned} \tag{12}$$

Similarly, when $t = t_i$ ($i$ = 3, 4 … $m$+1), $\boldsymbol{q}$ ($t_i$) can be represented by

$$\begin{aligned}\mathbf{q}(t_i) &= e^{\mathbf{A}(t_i-t_{i-1})}\mathbf{q}(t_{i-1}) + a_p\int_{t_{i-1}}^{t_i} e^{\mathbf{A}(t_i-\xi)}\mathbf{B}(\xi)[\mathbf{q}(\xi)-\mathbf{q}(\xi-T)]d\xi \\ &= e^{\mathbf{A}(t_i-t_{i-1})}\mathbf{q}(t_{i-1}) + \frac{\tau}{2}a_p\begin{Bmatrix} e^{\mathbf{A}(t_i-t_{i-1})}\mathbf{B}(t_{i-1})\left[\mathbf{q}(t_{i-1})-\mathbf{q}(t_{i-1}-T)\right]+ \\ \mathbf{B}(t_i)\left[\mathbf{q}(t_i)-\mathbf{q}(t_i-T)\right] \end{Bmatrix}\end{aligned} \tag{13}$$

Substituting Eqs. (11) - (13) into Eq. (4) yields the discrete map as follows:

$$(\mathbf{I}-\mathbf{D}_1-\frac{a_p\tau}{2}\mathbf{E}_1)\begin{bmatrix}\mathbf{q}(t_1)\\ \mathbf{q}(t_2)\\ \vdots \\ \mathbf{q}(t_{m+1})\end{bmatrix} = (\mathbf{F}_1-\frac{a_p\tau}{2}\mathbf{E}_1)\begin{bmatrix}\mathbf{q}(t_1\text{-}T)\\ \mathbf{q}(t_2\text{-}T)\\ \vdots \\ \mathbf{q}(t_{m+1}\text{-}T)\end{bmatrix} \tag{14}$$

with

$$\mathbf{D}_1 = \begin{bmatrix} 0 & & & & \\ e^{\mathbf{A}\tau} & 0 & & & \\ & e^{\mathbf{A}\tau} & 0 & & \\ & & \ddots & \ddots & \\ & & & e^{\mathbf{A}\tau} & 0 \end{bmatrix} \quad \mathbf{F}_1 = \begin{bmatrix} 0 & & \cdots & 0 & e^{\mathbf{A}T_f} \\ 0 & 0 & & 0 & 0 \\ & & \ddots & & \\ & & & 0 & \\ 0 & & & & 0 \end{bmatrix}$$

$$\mathbf{E}_1 = \begin{bmatrix} 0 & & & & \\ e^{\mathbf{A}\tau}\mathbf{B}_1 & \mathbf{B}_2 & & & \\ & e^{\mathbf{A}\tau}\mathbf{B}_2 & \mathbf{B}_3 & & \\ & & \ddots & \ddots & \\ & & & e^{\mathbf{A}\tau}\mathbf{B}_m & \mathbf{B}_{m+1} \end{bmatrix}$$

where $\boldsymbol{B}_i$ stands for $\boldsymbol{B}(t_i)$ ( $i$ =1, 2 ).

The transition matrix $\boldsymbol{\Phi}$ of the milling system over one time period $T$ can be obtained as

$$\boldsymbol{\Phi} = (\mathbf{I}-\mathbf{D}_1-\frac{a_p\tau}{2}\mathbf{E}_1)^{-1}(\mathbf{F}_1-\frac{a_p\tau}{2}\mathbf{E}_1) \tag{15}$$

Finally, the corresponding chatter stability can be predicted according to the Floquet theory. The obtained 1st INIM is equivalent to the NIM based on the Newton-Cotes formula built in Ref. [31].

3.2.2 Second-order INIM (2nd INIM)

The second-order numerical integral formula can be used to approximate the integral item of Eq. (4) as well. Similarly, at point $t_1$, $\boldsymbol{q}$ ($t_1$) is the same as that with the first-order INIM. Then, at time point

$t_2$, the value $\boldsymbol{q}$ ($t_2$) can be described as

$$\mathbf{q}(t_2)=e^{\mathbf{A}(t_2-t_1)}\mathbf{q}(t_1)+\frac{\tau}{12}a_p\begin{Bmatrix}5e^{\mathbf{A}(t_2-t_1)}\mathbf{B}(t_1)[\mathbf{q}(t_1)-\mathbf{q}(t_1-T)]+\\8\mathbf{B}(t_2)[\mathbf{q}(t_2)-\mathbf{q}(t_2-T)]-\\e^{\mathbf{A}(t_2-t_3)}\mathbf{B}(t_3)[\mathbf{q}(t_3)-\mathbf{q}(t_3-T)]\end{Bmatrix} \tag{16}$$

At $t=t_i$ ($i=3, 4 \ldots m$), the value $\boldsymbol{q}$ ($t_i$) can be expressed by

$$\mathbf{q}(t_i)=e^{\mathbf{A}(t_i-t_{i-1})}\mathbf{q}(t_{i-1})+\frac{\tau}{12}a_p\begin{Bmatrix}5e^{\mathbf{A}(t_i-t_{i-1})}\mathbf{B}(t_{i-1})[\mathbf{q}(t_{i-1})-\mathbf{q}(t_{i-1}-T)]+\\8\mathbf{B}(t_i)[\mathbf{q}(t_i)-\mathbf{q}(t_i-T)]-\\e^{\mathbf{A}(t_i-t_{i+1})}\mathbf{B}(t_{i+1})[\mathbf{q}(t_{i+1})-\mathbf{q}(t_{i+1}-T)]\end{Bmatrix} \tag{17}$$

However, Eq. (17) is not suitable for $\boldsymbol{q}$ ($t_{m+1}$) at $t=t_{m+1}$. This is because the time point $t=t_{m+2}$ does not appear. Therefore, $\boldsymbol{q}$ ($t_{m+1}$) should be approximated according to the first-order numerical integral formula, which can be given by

$$\mathbf{q}(t_{m+1})=e^{\mathbf{A}(t_{m+1}-t_m)}\mathbf{q}(t_m)+\frac{\tau}{2}a_p\begin{Bmatrix}e^{\mathbf{A}(t_{m+1}-t_m)}\mathbf{B}(t_m)[\mathbf{q}(t_m)-\mathbf{q}(t_m-T)]\\+\mathbf{B}(t_{m+1})[\mathbf{q}(t_{m+1})-\mathbf{q}(t_{m+1}-T)]\end{Bmatrix} \tag{18}$$

Combining Eqs. (11), (16), (17), and (18) to describe Eq. (4), the discrete map of the milling system can be performed as

$$(\mathbf{I}-\mathbf{D}_2-\frac{a_p\tau}{12}\mathbf{E}_2)\begin{bmatrix}\mathbf{q}(t_1)\\\mathbf{q}(t_2)\\\vdots\\\mathbf{q}(t_{m+1})\end{bmatrix}=(\mathbf{F}_2-\frac{a_p\tau}{12}\mathbf{E}_2)\begin{bmatrix}\mathbf{q}(t_1\text{-}T)\\\mathbf{q}(t_2\text{-}T)\\\vdots\\\mathbf{q}(t_{m+1}\text{-}T)\end{bmatrix} \tag{19}$$

with

$$\mathbf{D}_2=\begin{bmatrix}0&&&&\\e^{\mathbf{A}\tau}&0&&&\\&e^{\mathbf{A}\tau}&0&&\\&&\ddots&\ddots&\\&&&e^{\mathbf{A}\tau}&0\end{bmatrix}\quad\mathbf{F}_2=\begin{bmatrix}0&&\cdots&0&e^{\mathbf{A}T_f}\\0&0&&0&0\\&&\ddots&&\\&&&0&\\0&&&&0\end{bmatrix}$$

$$\mathbf{E}_2=\begin{bmatrix}0&&&&\\5e^{\mathbf{A}\tau}\mathbf{B}_1&8\mathbf{B}_2&-e^{-\mathbf{A}\tau}\mathbf{B}_3&&\\&\ddots&\ddots&\ddots&\\&&5e^{\mathbf{A}\tau}\mathbf{B}_{m-1}&8\mathbf{B}_m&-e^{-\mathbf{A}\tau}\mathbf{B}_{m+1}\\&&&6e^{\mathbf{A}\tau}\mathbf{B}_m&6\mathbf{B}_{m+1}\end{bmatrix}$$

where $\boldsymbol{B}_i$ stands for $\boldsymbol{B}(t_i)$ ( $i$ =1, 2, and 3 ).

The transition matrix $\boldsymbol{\Phi}$ of the milling system over one time period $T$ can be obtained as

$$\mathbf{\Phi} = (\mathbf{I} - \mathbf{D}_2 - \frac{a_p \tau}{12}\mathbf{E}_2)^{-1}(\mathbf{F}_2 - \frac{a_p \tau}{12}\mathbf{E}_2) \tag{20}$$

According to the Floquet theory, the chatter stability of the milling system can be identified.

In this paper, the first two order Lagrange integration formulas are used to estimate the integral term of Eq. (4), where the higher orders are not considered. It is because the trapezoidal rule used to express the last two points in Eq. (18) limits the increase of the local discretization error [45].

## 4 Comparison and verification

To demonstrate the calculated efficiency and precision of the proposed 2nd INIM, it is imperative compare with the existing methods including the zeroth-order SDM (0th SDM) [3], the first-order FDM (1st FDM) [4], the second-order FDM (2nd FDM) [19], the third-order FDM (3rd FDM) [21], the trapezoidal NIM (Trap-NIM) [31], and the Simpson NIM (Simp-NIM) [34]. The convergence rate and stability lobe diagrams via the single-DOF and two-DOF milling systems are calculated by using these calculated methods. The system parameters are used as listed in Table 1. The calculated programs are written and operated in MATLAB 2018a of a personal computer (Intel (R) Core (TM) i5, 2.3 GHz, and 6 GB).

**Table 1**. System parameters

| Term | Notation | Value |
|---|---|---|
| Natural frequency | $f_n$ | 922 Hz |
| Damping ratio | $\zeta$ | 1.1 % |
| Modal mass | $m_t$ | 0.03993 kg |
| Cutting force coefficients | $K_t$ | $6 \times 10^8$ N/m$^2$ |
| | $K_n$ | $2 \times 10^8$ N/m$^2$ |
| Tooth number | N | 2 |

### 4.1 Single DOF milling system

The local discretization error is proposed to reflect the convergence efficiency of the discretization techniques [17]. The change of the difference between the approximated value $\mu$ and the exact value $\mu_0$, i.e. convergence rate, can describe the local errors, where $\mu$ is the maximal critical eigenvalue of the transition matrix.

For single DOF milling system, the convergence rates by using the SDM, FDMs, and NIMs are calculated, which are similar to those in Fig. 3. The exact eigenvalue $\mu_0$ is also obtained using the S-FDM with $m$ = 200. Then, under the machining parameters, including down milling operation, a / D = 1, Ω = 5000 rpm, and the cutting depths with 0.2 mm, 0.5 mm, and 1 mm, the convergence rates for these calculated method are shown in Fig. 5. Compared with the SDM and FDMs, it can be found that the convergence rate for the S-INIM is faster. Additionally, when the approximation value $m$ is equal to the larger value under any cutting depth, the difference between $\mu$ and $\mu_0$ for the S-INIM is smaller than those for the SDM and FDMs, which usually means that the S-INIM has higher accuracy. For instance, in Fig. 5(a), when $m$ = 40, the difference value for the S-INIM is about 0.004, which is less than 0.022, 0.0137, 0.007 and 0.009 from the SDM and FDMs. In comparison with the other NIMs, the proposed S-INIM shows the better convergence rate as well. Furthermore, the convergence rate curves for the Simp-NIM show the server oscillation phenomenon, since there exists the large order difference of the truncation errors for the numerical methods used to estimate the state value.

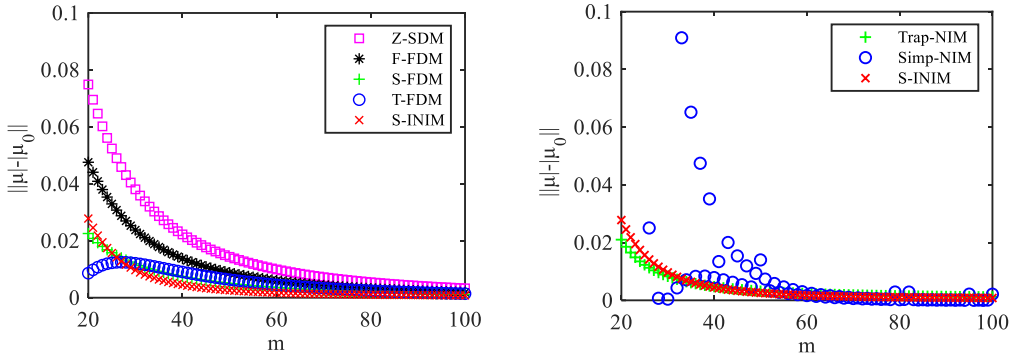


$a$ = 0.2 mm, $|\mu_0|$ = 0.8193

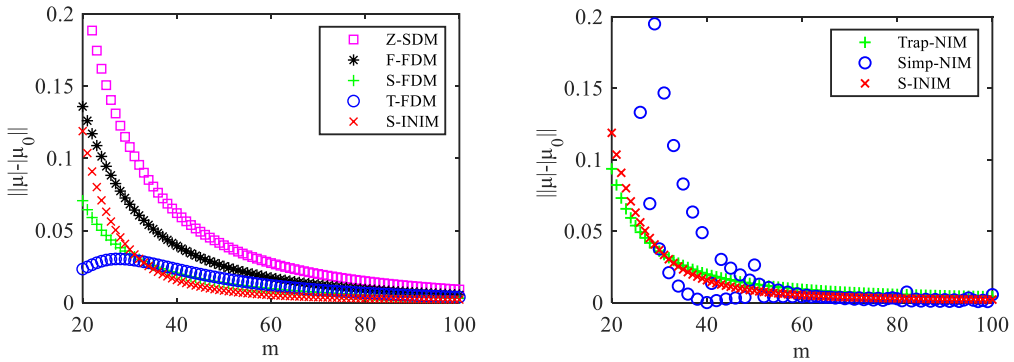


$a$ = 0.5 mm, $|\mu_0|$ = 1.0727

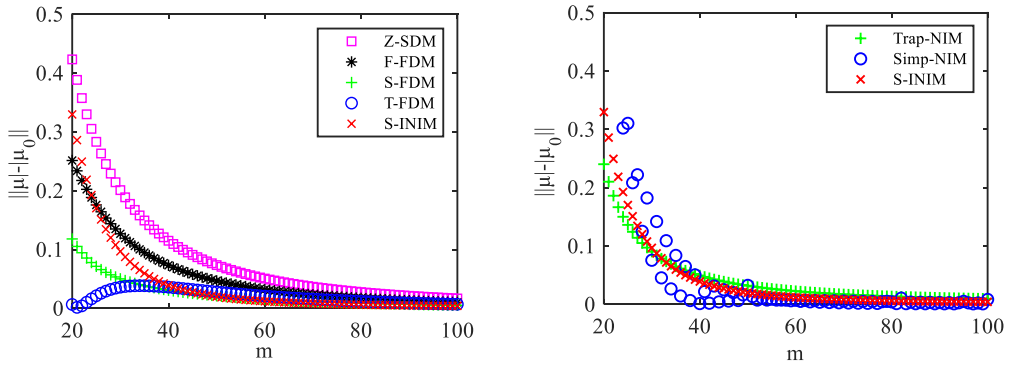


$a$ = 1 mm, $|\mu_0|$ = 1.4043

**Fig. 5** Convergence rate of the eigenvalues for changing approximate parameter $m$ for different methods.

Meantime, to further compare the computational accuracy, the SLDs are calculated by using the proposed S-INIM and the existing methods under different a / D and $m$. Therefore, Fig. 6 shows the SLDs under the spindle speed with the range of 5000 rpm < Ω < 10000 rpm. At a / D = 1, the red SLD for the S-INIM starts to be far from the ESB with black color, and then gradually gets close to the ESB when spindle speed increases. At a / D = 0.1 or 0.05, the SLD from the S-INIM is more near to the ESB than those from other methods as shown in Fig. 6(b) or 6(c), which indicates the accuracy of the S-INIM is higher.

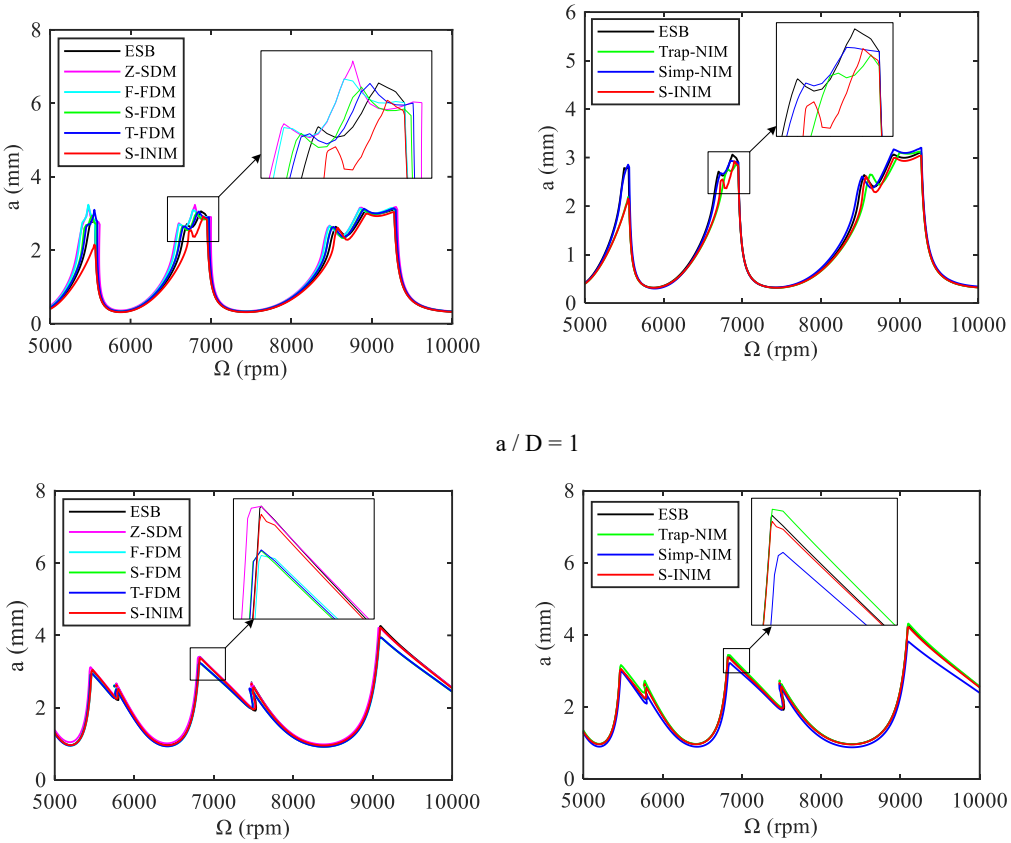


a / D = 1

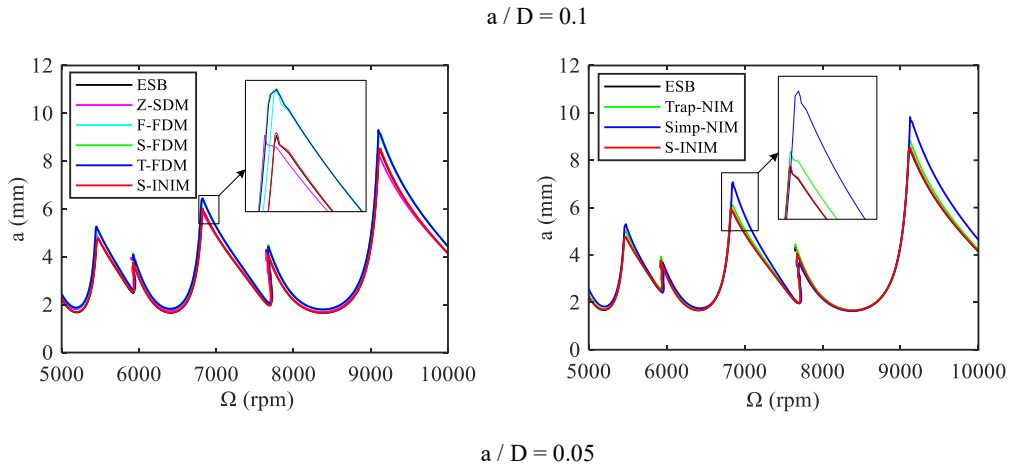


**Fig. 6** The SLDs for different methods under different a / D

When the approximation parameter *m* varies from 30, 50 to 80, the corresponding SLDs at a / D = 1 are also calculated using these predicted methods, which are shown in Fig. 7. When *m* is equal to 30, the SLD for the S-INIM is obviously far away from the ideal stability lobes, which appears at the other color SLDs as well. The phenomenon demonstrates the low accuracy of these methods with the small *m*. This can be observed from Fig. 5. The difference between $\mu$ and $\mu_0$ for the S-INIM is larger if *m* is chosen as small value, such as *m* = 30. When *m* = 50, the SLD for the S-INIM is near to the ESB with black color, and it is almost coincide with the ESB when *m* increases to 80. Thus, to improve the computational accuracy for predicting SLD, the time intervals should be selected with the larger value. However, the increasing *m* usually means the higher consumption of the computational time.

As shown in Fig. 8, the time cost for these different methods are compared under the change of *m* and a / D. Under any a / D, the runtime for the Z-SDM is more than other methods, and the computational time for the FDMs is more than for the NIMs. This conclusion is suitable for the condition of the varying *m*. With the increase of *m*, the computational time for all methods increases obviously, as seen in Fig. 8. For the NIMs, when *m* = 80, the runtime for the S-INIM with 142s slightly increases, compared with 133s and 137s for the Trap-NIM and Simp-NIM, respectively. That is to say, the proposed S-INIM shows better computational precision with just slightly loss of the computational efficiency.

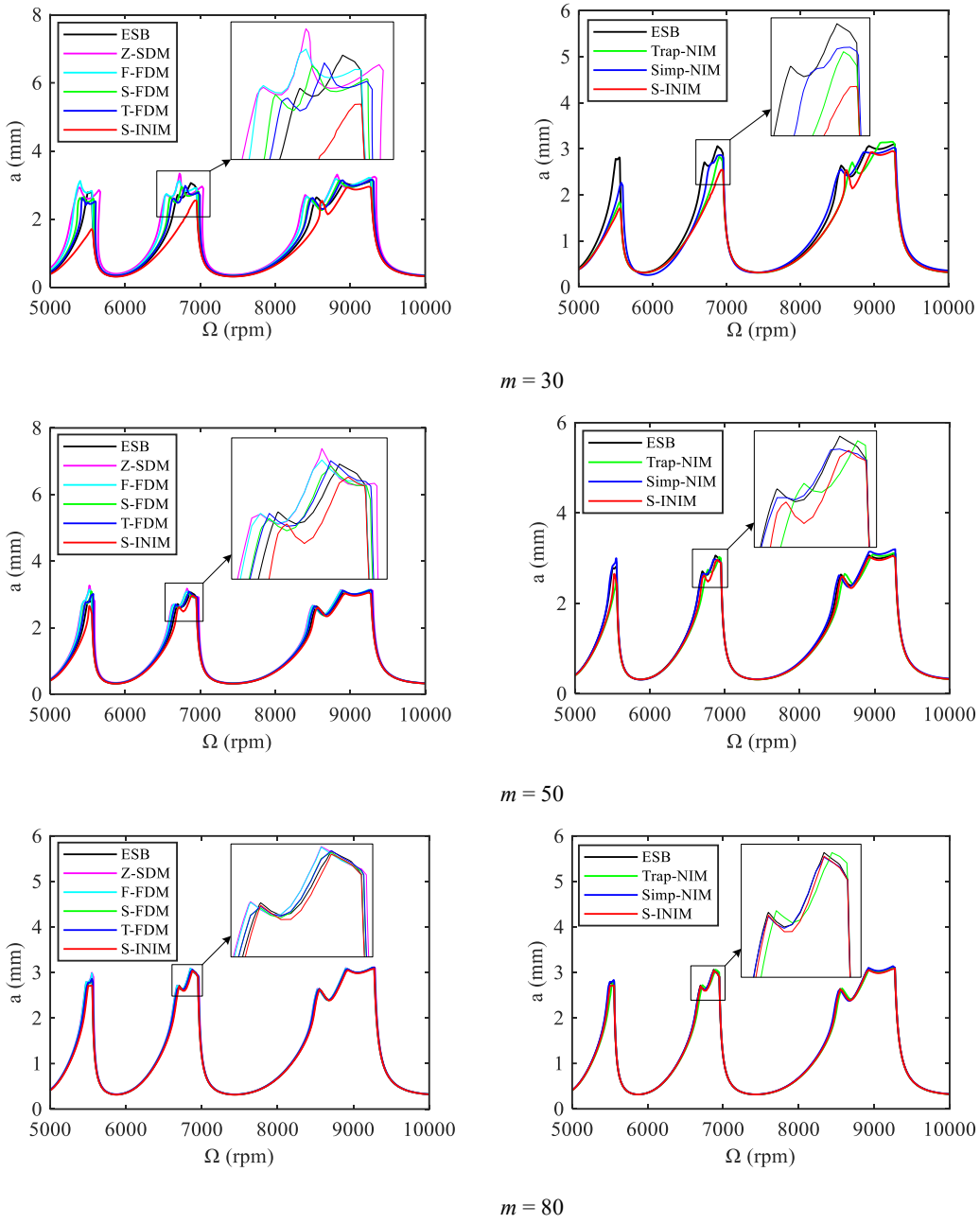


**Fig. 7** SLDs for different methods under different *m*.

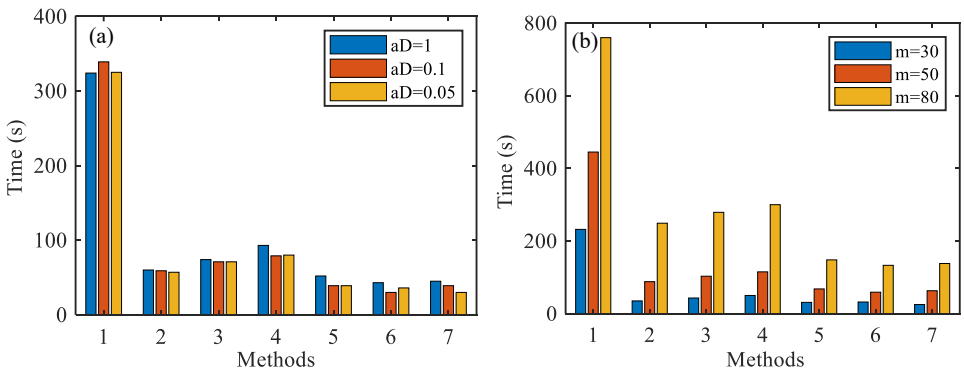


**Fig. 8** Comparison of the computational time for different methods. Here, number symbols from 1 to 7 refer

to the Z-SDM, F-FDM, S-FDM, T-FDM, S-INIM, Trap-NIM, and Simp-NIM, respectively.

### 4.2 Two DOF milling system

The proposed S-INIM can be applied to the two DOF milling system. In order to verify this, the stability prediction for the two DOF milling system in Fig. 1 is investigated, and the used system parameters are equal to those in the single DOF system, where the dynamic parameters along $x$ and $y$ directions are equal. Under the machining condition of up milling operation, a / D = 1, $\Omega$ = 5000 rpm, and the cutting depths with 0.2 mm, 0.5 mm, and 1 mm, the convergence rates using the proposed method and the existing ones are demonstrated in Fig. 9. It can be clearly observed that the S-INIM converges than the other methods. For instance, in Fig.9(c), when $m$ = 40 for the S-INIM, the difference between $\mu$ and $\mu_0$ is about 0.122. However, the corresponding $m$ for the Z-SDM, F-FDM, S-FDM, and T-FDM are 80, 98, 60, and 46, respectively. Although the $m$ for T-FDM is near to that for the S-INIM, the difference between $\mu$ and $\mu_0$ for T-FDM will increase when $m$ is larger than 49. Meantime, in Fig.9(c), compared with the Trap-NIM, the convergence rate for S-INIM will be better when m > 59. Hence, the proposed S-INIM has good prediction precision. In addition, there still exists the oscillation phenomenon of the convergence rate curve for the Simp-NIM, and meantime some jump points appear in the other curves.

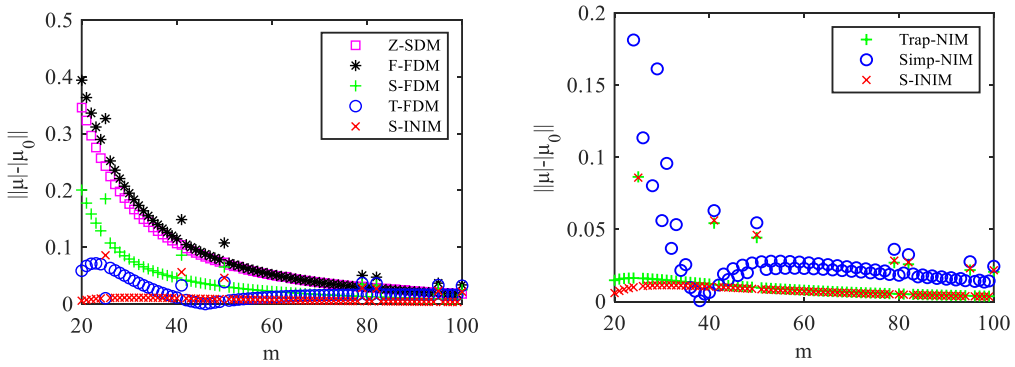


$a$ = 0.2 mm, $|\mu_0|$ = 2.1309

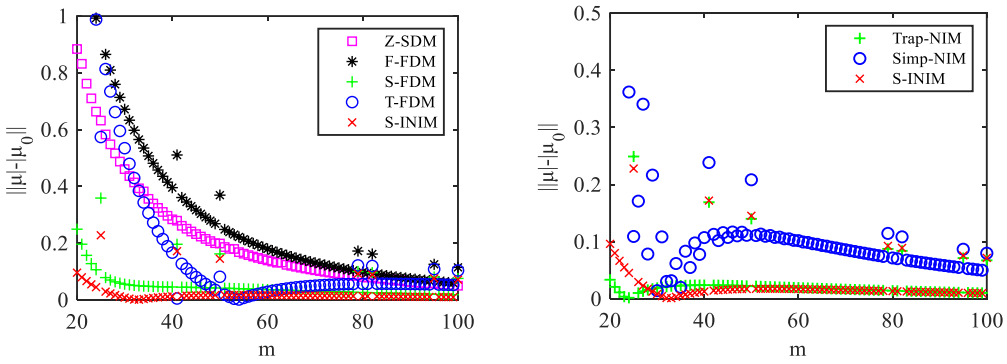

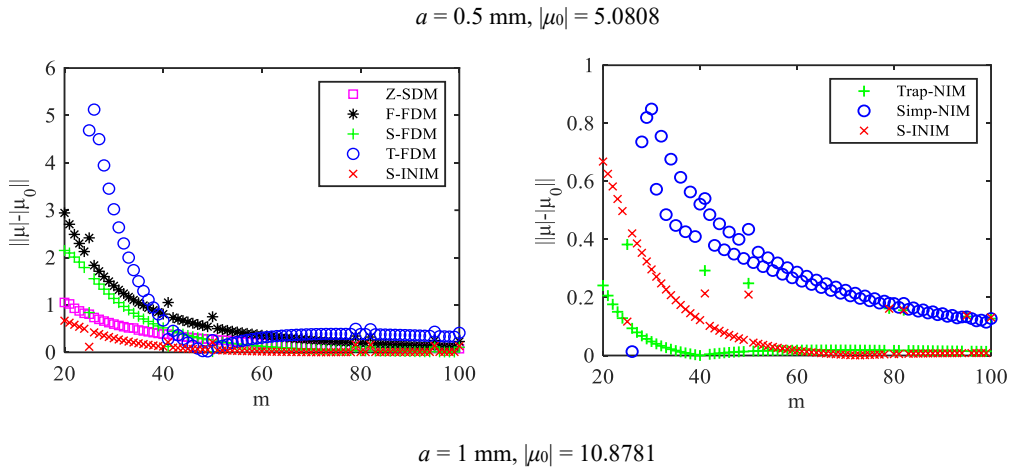


**Fig. 9** Convergence rate of the eigenvalues for changing approximate parameter *m* for different methods.

Figures 10 and 11 show the stability lobe diagrams for the S-INIM and the existing methods with the varying a / D and *m*, respectively. From Fig. 10, it can be seen that the SLD for the S-INIM is more close to the ESB with *m* = 200, whereas the lobes for the Z-SDM and Simp-NIM are far away from the ESB. Especially, in Fig. 10(c), i.e. a / D = 0.05, when the spindle speed increases from 5000 rpm to 10000 rpm, the shape of the stability lobes for the Simp-NIM gradually becomes different with that of the ESB, while the SLD for S-INIM is more close to the ESB. These analysis show that the proposed S-INIM has high accurate for predicting the stability charts of the two DOF milling system.

From the aspect of the number of time interval, when *m* = 30, the stability chart for the S-INIM has been near to the ESB, whereas the SLDs for Z-SDM and FDMs keep a certain distance with the ESB, which shows the high accuracy for the proposed S-INIM. As *m* increases, the accuracy of the predicted SLDs has been improved for these methods, but the computational times will be also increased obviously, which can be verified in Fig. 12(b). At the same time, it is clear in Fig. 12 that the computational time for the S-INIM just increases slightly, compared with the existing NIMs. In other words, when predicting the stability charts using the proposed S-INIM, the computational accuracy is improved under the little loss of the computational efficiency.

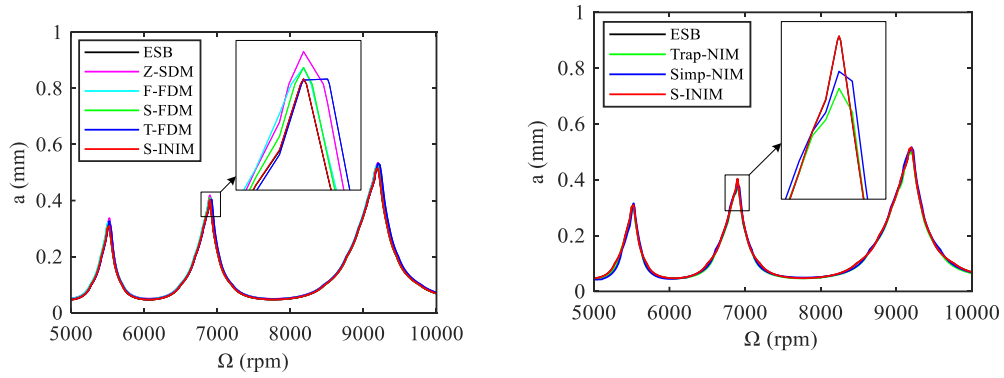


a / D = 1

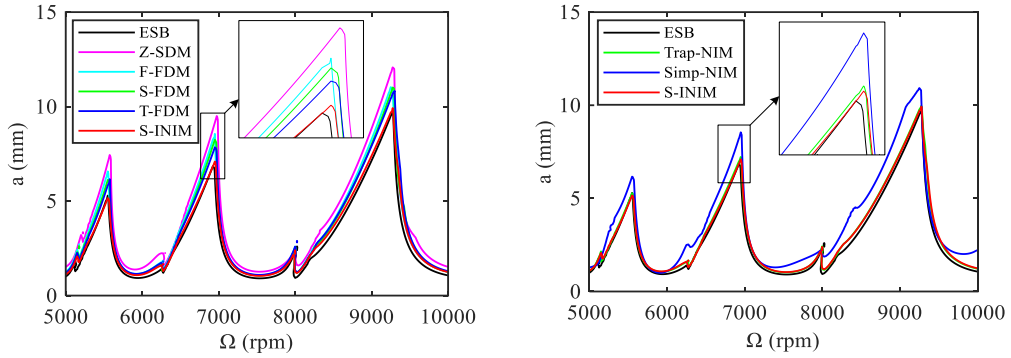


a / D = 0.1

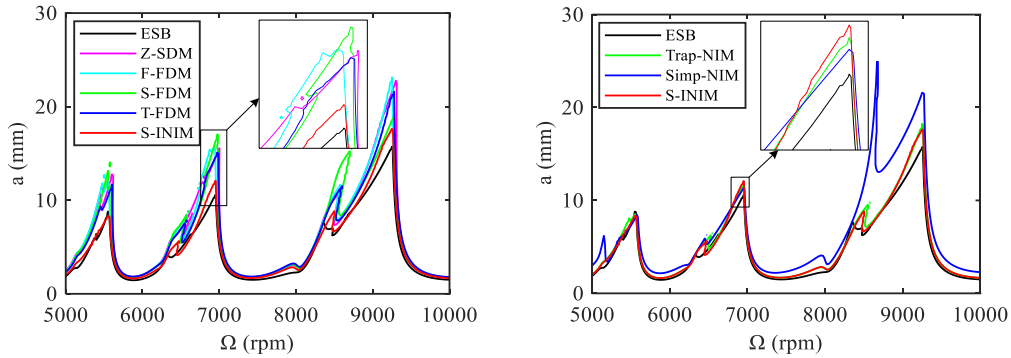


a / D = 0.05

**Fig. 10** SLDs for different methods under different a / D.

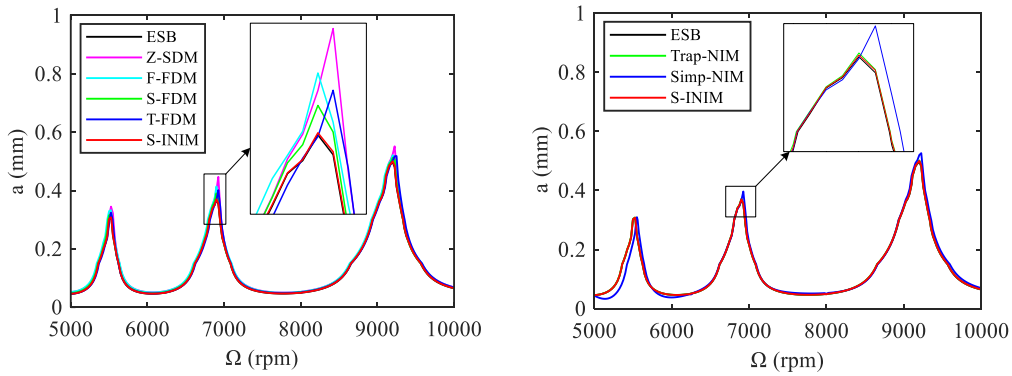

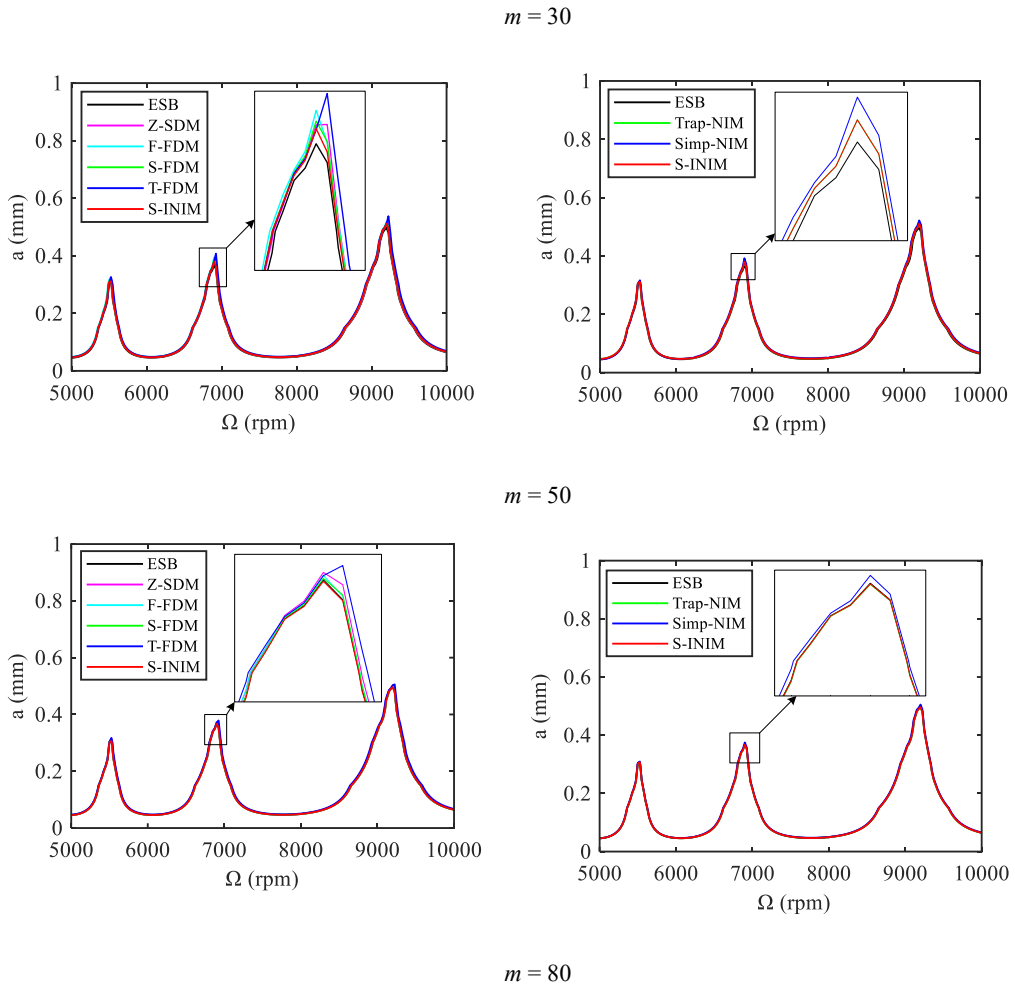


**Fig. 11** SLDs for different methods under different *m*.

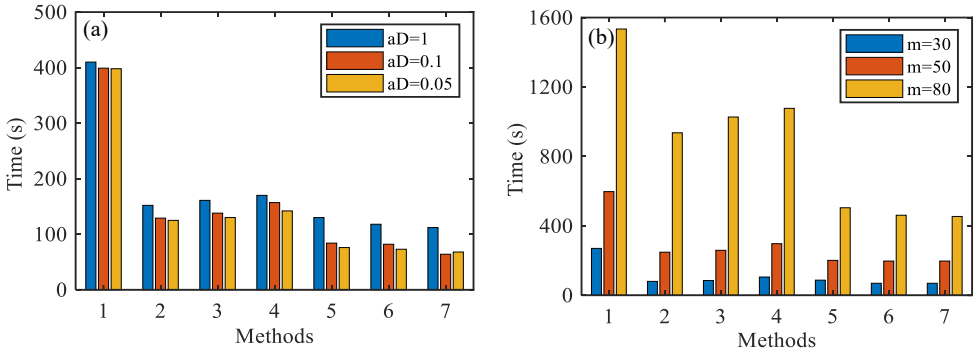


**Fig. 12** Comparison of the computational time for different methods. Here, number symbols from 1 to 7 refer to the Z-SDM, F-FDM, S-FDM, T-FDM, S-INIM, Trap-NIM, and Simp-NIM, respectively.

## 5 Conclusions

In this study, an improved numerical integration method for predicting the chatter stability is proposed based on the Lagrange interpolation scheme. Considering the regenerative effect, the dynamic model of the milling process is represented by the state equation with time delay, and the

response of the equation is described as the integral form by the direct integration method. By equally discretizing the forced vibration process of the time delay period into a series of small intervals, the first three order Lagrange numerical integration formulas are used over each small interval to approximate the integral item of the system response respectively, thereby building the improved numerical integration methods (INIMs). On this basis, the milling stability is predicted from the constructed state transition matrix of the system using the Floquet theory. After comparison analysis, it is proved that the second order INIM is optimal.

The single and two DOF milling systems are illustrated to predict the convergence rates and the stability lobes by using the existing SDM, FDMs, NIMs, and the proposed INIM, respectively. It is found that the INIM convergences faster than the others, even though its difference between the approximated value and the exact value is not smallest under the small number of the approximation parameter. The analysis of the stability lobes shows that the accuracy and efficiency of the proposed INIM is higher than those for the SDM and FDMs. In comparison with the existing NIMs, the proposed INIM could take just slightly more computational time, but has greater computational precision.

**Funding information** This research was funded by National Natural Science Foundation of China (Grant No. 51975336), Key Research and Development Program of Shandong Province (Grant No. 2019JZZY010112), Key Basic Research Project of Natural Science Foundation of Shandong Province (Grant No. ZR2018ZB0106).

**Conflict of interest** The authors declare that they have no conflict of interest.

**Availability of data and material** Not applicable

**Code availability** Not applicable

**Authors' contributions** Yi Wan, Xichun Luo and Zhanqiang Liu contributed to the conceptualization and methodology; Yan Xia and Qinghua Song performed the investigation and analysis; Yan Xia wrote the manuscript.

**Appendix. Coefficient matrixes for single and two DOF milling systems**

The coefficient matrixes for the single DOF milling system can be described as

$$\mathbf{A}=\begin{bmatrix} -\xi\omega_n & \dfrac{1}{m_t} \\ (\xi^2-1)m_t\omega_n^2 & -\xi\omega_n \end{bmatrix}$$

$$\mathbf{B}(t)=\begin{bmatrix} 0 & 0 \\ h(t) & 0 \end{bmatrix}$$

where $h(t)$ is the cutting force coefficient.

The coefficient matrixes for the two DOF milling system can be described as

$$\mathbf{A}=\begin{bmatrix} -\mathbf{M}^{-1}\mathbf{C}/2 & \mathbf{M}^{-1} \\ \mathbf{C}\mathbf{M}^{-1}\mathbf{C}/4-\mathbf{K} & -\mathbf{C}\mathbf{M}^{-1}/2 \end{bmatrix}$$

$$\mathbf{B}(t)=\begin{bmatrix} 0 & 0 & 0 & 0 \\ 0 & 0 & 0 & 0 \\ h_{xx}(t) & h_{xy}(t) & 0 & 0 \\ h_{yx}(t) & h_{yy}(t) & 0 & 0 \end{bmatrix}$$

with

$$\mathbf{M}=\begin{bmatrix} m_t & \\ & m_t \end{bmatrix} \quad \mathbf{C}=\begin{bmatrix} 2m_t\xi & \\ & 2m_t\xi \end{bmatrix} \quad \mathbf{K}=\begin{bmatrix} m_t\omega_n^2 & \\ & m_t\omega_n^2 \end{bmatrix}$$

**References**


1. Zhu LD, Liu CF (2020) Recent progress of chatter prediction, detection and suppression in milling. Mech Syst Signal Process 143:106840.
2. Altintas Y (2000) Manufacturing automation, metal cutting mechanics, Machine Tool Vibrations, and CNC Design. Cambridge University Press, USA.
3. Insperger T, Stépán G (2004) Updated semi-discretization method for periodic delay-differential equations with discrete delay. Int J Numer Meth Eng 61:117-141.
4. Ding Y, Zhu LM, Zhang XJ, Ding H (2010) A full-discretization method for prediction of milling stability. Int J Mach Tools Manuf 50(5):502-509.
5. Kakinuma Y, Sudo Y, Aoyama T (2011) Detection of chatter vibration in end milling applying disturbance observer. CIRP Annals 60(1): 109-112.
6. Lamraoui M, Thomas M, El Badaoui M (2014) Cyclostationarity approach for monitoring chatter and tool wear in high speed milling. Mech Syst Signal Process 44(1): 177-198.
7. Fallah M, Moetakef-Imani B (2019) Adaptive inverse control of chatter vibrations in internal turning operations. Mech Syst Signal Process 129: 91-111.
8. Xia Y, Wan Y, Luo XC, Wang HW, Gong N, Cao JL, Liu ZQ, Song QH (2020) Development

of a toolholder with high dynamic stiffness for mitigating chatter and improving machining efficiency in face milling. Mech Syst Signal Process 145: 106928.

9. Altintaş Y, Budak E (1995) Analytical prediction of stability lobes in milling. CIRP Annals 44(1): 357-362.
10. Budak E, Altintas Y (1998) Analytical prediction of chatter stability in milling—part I: general formulation. J Dyn Sys Meas Control 120(1): 22-30.
11. Merdol D, Altintas Y (2004) Multi frequency solution of chatter stability for low immersion milling. J Manuf Sci Eng 126(3): 459-466.
12. Altıntas Y, Engin S, Budak E (1999) Analytical stability prediction and sesign of variable pitch cutters. J Manuf Sci Eng 121(2): 173-178.
13. Turner S, Merdol D, Altintas Y, Ridgway K (2007) Modelling of the stability of variable helix end mills. Int J Mach Tools Manuf 47(9): 1410-1416.
14. Tlusty J, Zaton W, Ismail F (1983) Stability lobes in milling. CIRP Annals 32(1): 309-313.
15. Bayly PV, Halley JE, Mann BP, Davies MA (2003) Stability of interrupted cutting by temporal finite element analysis. J Manuf Sci Eng 125(2): 220-225.
16. Li ZQ, Liu Q (2008) Solution and analysis of chatter stability for end milling in the time-domain. Chin J Aeronaut 21(2): 169-178.
17. Insperger T (2010) Full-discretization and semi-discretization for milling stability prediction: some comments. Int J Mach Tools Manuf 50(7): 658-662.
18. Jiang SL, Sun YW, Yuan XL, Liu WR (2017) A second-order semi-discretization method for the efficient and accurate stability prediction of milling process. Int J Adv Manuf Technol 92(1): 583-595.
19. Ding Y, Zhu LM, Zhang XJ, Ding H (2010) Second-order full-discretization method for milling stability prediction. Int J Mach Tools Manuf 50(10): 926-932.
20. Tang XW, Peng FY, Yan R, Gong YH, Li YT, Jiang LL (2017) Accurate and efficient prediction of milling stability with updated full-discretization method. Int J Adv Manuf Technol 88(9): 2357-2368.
21. Quo Q, Sun YW, Jiang Y (2012) On the accurate calculation of milling stability limits using third-order full-discretization method. Int J Mach Tools Manuf 62:61-66.

22. Yan ZH, Wang XB, Liu ZB, Wang DQ, Jiao L, Ji YJ (2017) Third-order updated full-discretization method for milling stability prediction. Int J Adv Manuf Technol 92: 2299-2309.
23. Yang WA, Huang C, Cai XL, You YP (2020) Effective and fast prediction of milling stability using a precise integration-based third-order full-discretization method. Int J Adv Manuf Technol 106(9): 4477-4498.
24. Xia Y, Wan Y, Luo XC, Liu ZQ, Song QH (2020) Milling stability prediction based on the hybrid interpolation scheme of the Newton and Lagrange polynomials. Int J Adv Manuf Technol 112: 1501-1512.
25. Liu YL, Zhang DH, Wu BH (2012) An efficient full-discretization method for prediction of milling stability. Int J Mach Tools Manuf 63: 44-48.
26. Ji YJ, Wang XB, Liu ZB, Wang HJ, Yan ZH (2018) An updated full-discretization milling stability prediction method based on the higher-order Hermite-Newton interpolation polynomial. Int J Adv Manuf Technol 95(5): 2227-2242.
27. Ozoegwu CG, Omenyi SN, Ofochebe SM (2015) Hyper-third order full-discretization methods in milling stability prediction. Int J Mach Tools Manuf 92: 1-9.
28. Zhou K, Feng PF, Xu C, Zhang JF, Wu ZJ (2017) High-order full-discretization methods for milling stability prediction by interpolating the delay term of time-delayed differential equations. Int J Adv Manuf Technol 93(5):2201-2214.
29. Li MZ, Zhang GJ, Huang Y (2013) Complete discretization scheme for milling stability prediction. Nonlinear Dyn 71(1): 187-199.
30. Li ZQ, Yang ZK, Peng YR, Zhu F, Ming XZ (2016) Prediction of chatter stability for milling process using Runge-Kutta-based complete discretization method. Int J Adv Manuf Technol 86(1): 943-952.
31. Ding Y, Zhu LM, Zhang XJ, Ding H (2011) Numerical integration method for prediction of milling stability. J Manuf Sci Eng 133(3): 1-9.
32. Zhang XJ, Xiong CH, Ding Y, Feng MJ, Xiong YL (2012) Milling stability analysis with simultaneously considering the structural mode coupling effect and regenerative effect. Int J Mach Tools Manuf 53(1): 127-140.
33. Zhang Z, Li HG, Meng G, Liu C (2015) A novel approach for the prediction of the milling

stability based on the Simpson method. Int J Mach Tools Manuf 99：43-47.

34. Zhang XJ, Xiong CH, Ding Y, Ding H (2017) Prediction of chatter stability in high speed milling using the numerical differentiation method. Int J Adv Manuf Technol 89(9-12)： 2535-2544.
35. Mei YG, Mo R, Sun HB, He BB, Wan N (2019) Stability prediction in milling based on linear multistep method. Int J Adv Manuf Technol 105(5): 2677-2688.
36. Qin CJ, Tao JF, Li L, Liu CL (2017) An Adams-Moulton-based method for stability prediction of milling processes. Int J Adv Manuf Technol 89(9): 3049-3058.
37. Dun YC, Zhu LD, Wang SH (2020) Multi-modal method for chatter stability prediction and control in milling of thin-walled workpiece. Appl Math Model 80: 602-624.
38. Zhi HY, Zhang TS, Du J, Yan XG (2020) An efficient full-discretization method for milling stability prediction. Int J Adv Manuf Technol 107(11-12): 4955-4967.
39. Balachandran B, Zhao MX (2000) A mechanics based model for study of dynamics of milling operations. Meccanica 35(2): 89-109.
40. Balachandran B (2001) Nonlinear dynamics of milling processes. Phil Trans R Soc Lond A 359:793-819.
41. Balachandran B, Gilsinn D (2005) Non-linear oscillations of milling. Math Comp Model Dyn 11(3): 273-290.
42. Balachandran B, Kalmar-Nagy T, Gilsinn D (2009) Delay differential equations recent advances and new directions. Springer, New York
43. Ding Y, Niu JB, Zhu LM, Ding H (2016) Numerical integration method for stability analysis of milling with variable spindle speeds. ASME J Vib Acoust 138: 1-11.
44. Niu JB, Ding Y, Zhu LM, Ding H (2016) Stability analysis of milling processes with periodic spindle speed variation via the variable-step numerical integration method. J Manuf Sci Eng Trans ASME 138:1-11.
45. Zhang XJ, Xiong CH, Ding Y, Ding H. Updated numerical integration method for stability calculation of Mathieu equation with various time delays [J]. Nonlinear Dynamics, 2017, 87(4): 2077-2095.